NANO LETTERS

pubs.acs.org/NanoLett Letter

Formation of In-Plane Semiconductor−Metal Contacts in 2D Platinum Telluride by Converting $PtTe_2$ to Pt_2Te_2

Kinga Lasek,[⊥] Jingfeng Li,[⊥] Mahdi Ghorbani-Asl, Salma Khatun, Onyedikachi Alanwoko, Vimukthi Pathirage, Arkady V. Krasheninnikov, and Matthias Batzill*

Cite This: Nano Lett. 2022, 22, 9571−9577 Read Online

ACCESS | Metrics & More | Article Recommendations | Supporting Information

ABSTRACT: Monolayer $PtTe_2$ is a narrow gap semiconductor while Pt_2Te_2 is a metal. Here we show that the former can be transformed into the latter by reaction with vapor-deposited Pt atoms. The transformation occurs by nucleating the Pt_2Te_2 phase within $PtTe_2$ islands, so that a metal−semiconductor junction is formed. A flat band structure is found with the Fermi level of the metal aligning with that of the intrinsically p-doped $PtTe_2$. This is achieved by an interface dipole that accommodates the ∼0.2 eV shift in the work functions of the two materials. First-principles calculations indicate that the origin of the interface dipole is the atomic scale charge redistributions at the heterojunction. The demonstrated compositional phase transformation of a 2D semiconductor into a 2D metal is a promising approach for making in-plane metal contacts that are required for efficient charge injection and is of particular interest for semiconductors with large spin−orbit coupling, like $PtTe_2$.

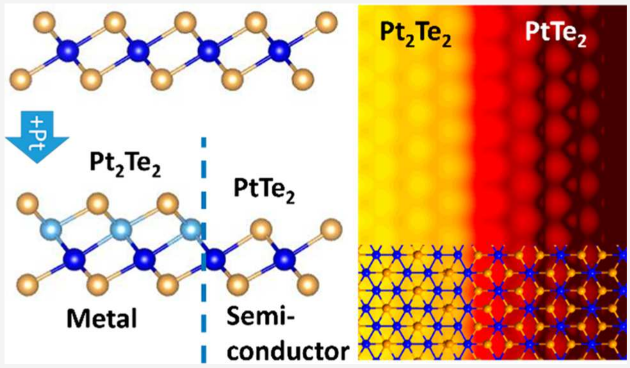

KEYWORDS: *2D materials, phase change, metal−semiconductor junction, platinum telluride*

Phase transformations in 2D materials and development of heterostructures based on the compounds with the same chemical composition have recently received considerable attention due to the possibility of postsynthesis modifications of existing structures. In particular, switching between semiconducting and metallic phases of 2D sheets of transition metal dichalcogenides (TMDs) has been accomplished by structural phase changes from the 2H-semiconducting to the 1T′-metallic phase in group VIB TMDs.[1] Such phase transformations can be achieved by increasing vacancy concentration due to thermal treatment,[2] electron irradiation,[3] or charge doping by alkali metal atom adsorption.[4−8] Since in most cases a structural switch occurs from the lower energy H-phase to a higher energy T′-phase,[9,10] these transformations are reversible, and the system can return back to the more stable H-phase. In contrast, compositional phase changes in 2D materials[11−13] are not spontaneously reversible, and thus the produced phases are stable. However, there are few examples of compositional control of contacts, and usually these are mixtures of 2D and 3D crystal structures.[14]

$PtTe_2$ is an intriguing material with strongly layer dependent electronic properties. Only the monolayer is semiconducting, while multilayers and bulk materials are metallic.[15] Moreover, the platinum−tellurium system exhibits various layered compositional phases, including $PtTe_2$ and Pt_2Te_2.[16−19] While monolayer $PtTe_2$ is semiconducting with a band gap of ∼0.5 eV,[15] Pt_2Te_2 is metallic. Both phases possess a hexagonal structure with very closely matched lattice constants, so that a heterojunction between the two phases can be constructed with virtually no interface strain and defects. Here we demonstrate a low temperature process that enables the transformation of $PtTe_2$ into Pt_2Te_2 by incorporation of vapor deposited Pt atoms into the $PtTe_2$ monolayer. The partially converted monolayer flakes exhibit $PtTe_2/Pt_2Te_2$ heterojunctions, which enables the spectroscopic analysis of the semiconductor/metal interface in a planar system. In contrast to previous modifications of TMDs with excess transition metal atoms,[20−23] we consider here stable extended 2D phases, i.e., the transformation from one known 2D phase to a 2D phase with another stoichiometry of the same elements. The transformation of $PtTe_2$ to Pt_2Te_2 may be referred to as an introduction of an additional layer of Pt as schematically illustrated in Figure 1, without the need for rearrangement of the Pt atoms in $PtTe_2$. This close structural relationship between $PtTe_2$ and Pt_2Te_2 is expected to facilitate a

Received: September 21, 2022
Revised: November 15, 2022
Published: November 18, 2022

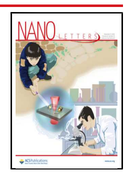

https://doi.org/10.1021/acs.nanolett.2c03715
Nano Lett. 2022, 22, 9571−9577

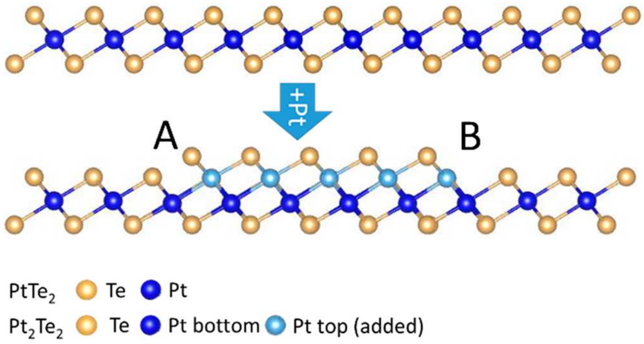

Figure 1. Schematic illustration of the phase transformation of $PtTe_2$ to Pt_2Te_2 by adding Pt atoms. $PtTe_2$ has a 1T-TMD structure, and the Pt_2Te_2 phase has two layers of Pt in between the tellurium layers. For partial transformation of a $PtTe_2$ layer, two kinds of phase boundaries between the $PtTe_2$ and Pt_2Te_2 phases can be formed along the zigzag direction of the 1T structure. These two phase boundaries are labeled "A" and "B".

compositional transformation by incorporation of excess Pt and the formation of well-defined heterojunctions.

$PtTe_2$ was grown by molecular beam epitaxy. This approach has been shown by several groups to result in high quality $PtTe_2$ films down to monolayer thickness if grown at low (250 °C) temperatures.[24,25] Growth at temperatures above 300 °C favors formation of bilayer thick islands.[26] Figure 2 shows the as grown $PtTe_2$ film, that consists of both mono- and bilayer islands. The Pt-4f XPS spectrum shows a single doublet, which is consistent with a single $PtTe_2$ phase sample.[15] The sample was then exposed to Pt vapor at 200 °C. The results of the STM and XPS measurements with increasing Pt exposure are also shown in Figure 2. In the STM images, the Pt_2Te_2 phase can be distinguished from the $PtTe_2$ phase by a difference of their layer heights as indicated in the line profiles. The Pt_2Te_2 phase is imaged as being 0.2−0.3 nm thicker than the $PtTe_2$ phase. In addition to the contrast change in STM images, the nucleation and growth of Pt_2Te_2 by reaction of $PtTe_2$ with Pt can also be followed in XPS. The two phases have distinct Pt-4f peaks with a chemical shift of ∼1.2 eV between the two phases.[15] Figure 2 also shows the variation of the Pt-4f components with increasing exposure. It is apparent that the component assigned to $PtTe_2$ decreases while the Pt_2Te_2 component increases, indicating the transformation of $PtTe_2$

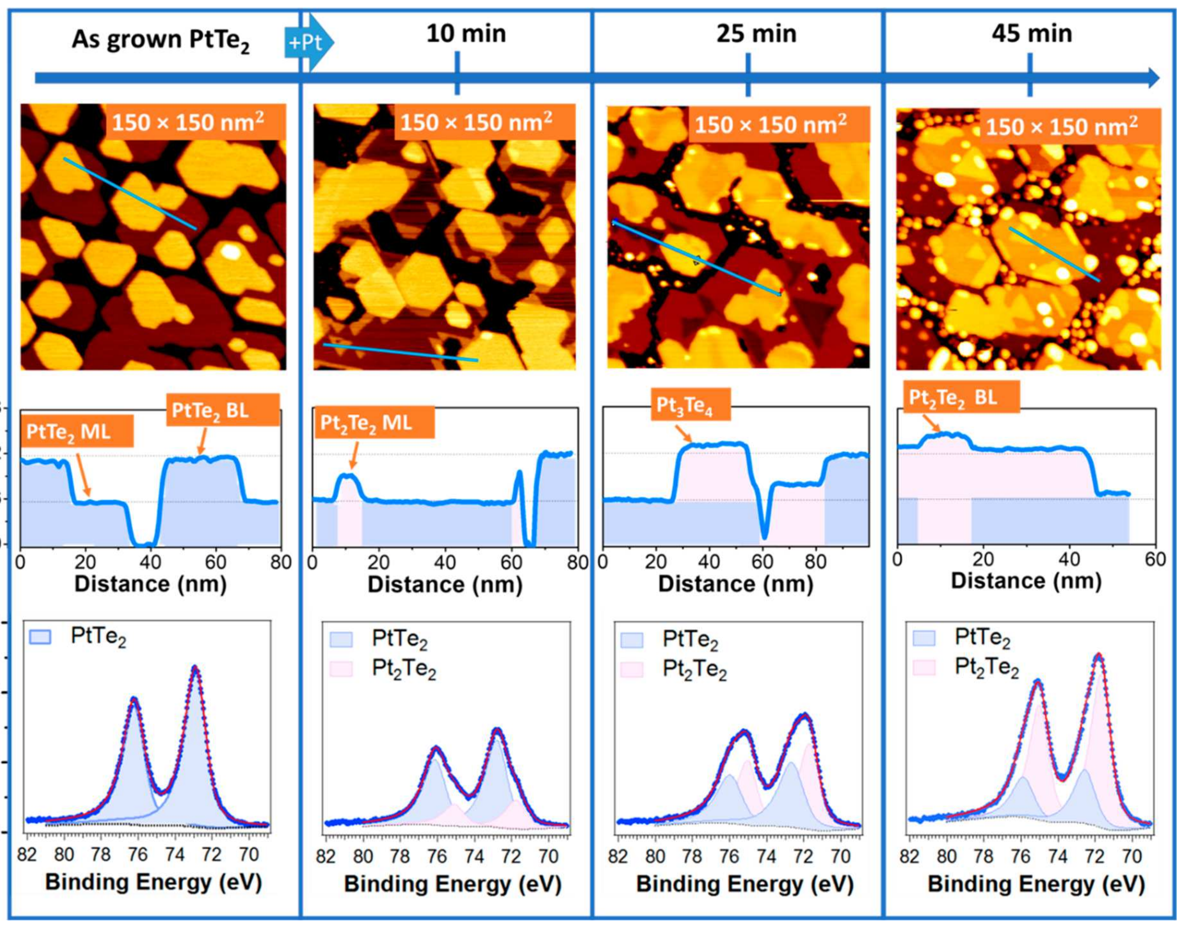

Figure 2. Sample evolution in STM and XPS with increasing Pt deposition. STM images and indicated line profiles show the conversion of $PtTe_2$ into Pt_2Te_2. The deposition of Pt on the sample is indicated on the top. Pt was deposited at a rate of ∼0.01 nm/min. The as grown $PtTe_2$ sample exhibits both mono- and bilayer $PtTe_2$ islands that convert into Pt_2Te_2 as Pt is deposited. The Pt_2Te_2 phase exhibits slightly higher contrast as evident in the STM images and highlighted by the line profile. In the line profiles the different phases are indicated by light blue for $PtTe_2$ and light pink for Pt_2Te_2 regions. For higher Pt exposures, Pt clusters are observed to form on the surface and the bare substrate region between the Pt−telluride islands. The conversion of $PtTe_2$ to Pt_2Te_2 is also observed in the Pt-4f core levels measured by XPS and shown at the bottom of the image for different Pt exposures. The Pt-4f is fitted with two doublets with the color of the components corresponding to Pt in a $PtTe_2$ environment (blue) and Pt_2Te_2 environment (pink).

https://doi.org/10.1021/acs.nanolett.2c03715
Nano Lett. 2022, 22, 9571−9577

to Pt_2Te_2. However, the transformation is incomplete, and some $PtTe_2$ remains on the surface. From STM images it is apparent that the monolayer has completely transformed so that the remaining $PtTe_2$ observed in XPS is likely due to second layer $PtTe_2$ in the bilayer regions. The STM images also reveal the nucleation of Pt clusters on the surface with increasing Pt deposition. Initially these clusters are primarily present in between Pt−telluride islands on the bare substrate. Once the Pt−telluride has transformed to Pt_2Te_2, Pt clusters also nucleate on the Pt_2Te_2 terraces. This suggests that vapor deposited Pt preferably incorporates into the $PtTe_2$ phase and only nucleates Pt clusters once all the $PtTe_2$ is converted into Pt_2Te_2.

First-principles calculations support the observed transformation processes. Excess Pt adsorbed on the surface of $PtTe_2$ strongly interacts with the system, giving rise to the destabilization of the Pt−Te bonds in the $PtTe_2$ phase (shown in Figure S1). Such a distortion of $PtTe_2$ by excess Pt shows that Pt will strongly react with the substrate and form "distorted" structures shown in Figure S1b. For a certain concentration of Pt added to $PtTe_2$, the Pt_2Te_2 phase can form, which is the lowest energy structure for this composition. Specifically, using appropriate Pt chemical potentials, our calculations show that formation of Pt_2Te_2 is favored over the nucleation of metallic Pt clusters, as illustrated in Figure S2. Moreover, Pt diffusion barriers on $PtTe_2$ have been calculated to be around 260 meV (Figure S1c). A low diffusion barrier facilitates the growth of the Pt_2Te_2 phase from a few nucleation sites in $PtTe_2$ islands. Further inspections of the STM images indicate that the Pt_2Te_2 preferentially nucleates at one edge orientation of the hexagonal $PtTe_2$ islands as shown in Figure 3. For extended islands, nucleation and growth of Pt_2Te_2 phases are sometimes observed on terraces. To illustrate nucleation sites, additional STM data are shown in Figure S3. The nucleation sites for the latter are not known, i.e., if it is homogeneous or heterogeneous nucleation. Nucleation density may be sensitively dependent on the kinetic parameters of deposition rate and sample temperature, and these parameters have not been systematically varied in this study. The Pt_2Te_2 phase has generally a triangular shape within the $PtTe_2$ phase. Preferred edge nucleation and Pt_2Te_2 domain shape indicate that there is an energetically preferred phase boundary between Pt_2Te_2 and $PtTe_2$. DFT calculations of the phase boundaries suggest that the phase boundary labeled "B" in Figure 1 is energetically preferred and thus is expected to be observed in the experiments.

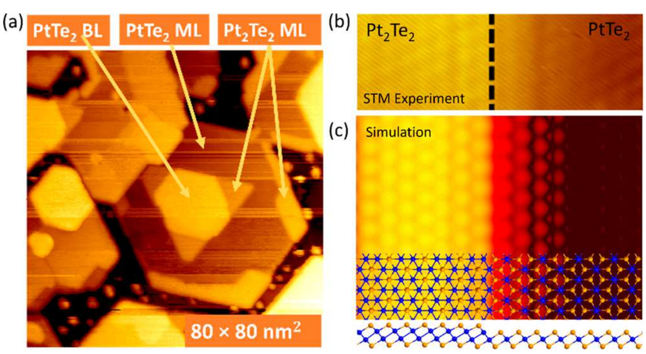

Figure 3. STM of Pt_2Te_2/$PtTe_2$ phase coexistence. (a) STM image of a partial conversion of $PtTe_2$ into the Pt_2Te_2 phase. It is apparent that the initial $PtTe_2$ islands have hexagonal shapes. For the monolayer 1T phase the two zigzag edges are identical if the substrate does not play an important role, and thus a hexagonal shape is expected. Formation of Pt_2Te_2, however, preferentially occurs at only one of the two edges. Similarly, Pt_2Te_2 embedded within the $PtTe_2$ phase island forms preferentially triangularly shaped Pt_2Te_2 phases. As shown in Figure 1, two different phase boundaries exist, and the preference of one phase boundary over another explains the orientation of the phase boundaries in the STM image. (b) Atomically resolved STM image of the interface. (c) Simulated STM image of the interface.

Making efficient electronic contacts to 2D semiconductors remains a challenge[27−30] with covalently bonded in-plane side contacts generally considered to allow for better charge injections as compared to metal top contacts, because top contacts exhibit an inevitable tunnel barrier across the van der Waals gap that increases the contact resistance.[31] High quality covalently bonded side contacts of metals to 2D materials are, however, much more challenging to engineer and thus have mostly been studied by theoretical calculations.[28] Detailed atomic-scale characterization and assessments of electronic properties of such side contacts are absent. The phase transformation of $PtTe_2$ into Pt_2Te_2 described above suggests that Pt-deposition onto $PtTe_2$ would not result in just a top contact to $PtTe_2$, but instead a transformation of $PtTe_2$ into Pt_2Te_2 occurs even at low deposition temperatures. This implies the formation of a side contact of semiconducting monolayer $PtTe_2$ with a metallic Pt_2Te_2 phase. The structural similarity between the two phases ensures an atomically sharp contact and absence of dislocation-type defects at the interface, as the STM images of the phase contact indicate. The controlled formation of this phase contact enables us to study the electronic structure of such a 2D metal/semiconductor side contact. In contrast to traditional buried metal/semiconductor contacts, the purely 2D lateral contact is exposed to vacuum and thus can be investigated by scanning tunneling spectroscopy. To obtain the interface band alignment, both the position of the band edges relative to the Fermi level and the work function (WF) alignment across the interface need to be determined. The former is measured directly by $I-V$ (dI/dV) spectroscopy, while the WF differences across the interface can be assessed by field emission resonance (FER) measurements. FER spectroscopy has been widely used to determine WF modulations in 2D monolayer materials on metal substrates, e.g., for hex-BN,[32,33] graphene,[34] oxide layers,[35,36] NaCl,[37] or CuN.[38] Briefly, in FER the bias voltage between an STM tip and the sample surface is chosen such that the Fermi level of the STM tip lies above the vacuum level of the sample. The drop of the potential in the tunnel junction gives rise to a triangular potential well between the tip and the sample surface with discrete image potential states that are probed in the FER spectroscopy. Local changes in the substrate WF shifts these image potential states corresponding to the WF changes and thus a shift of the resonance states is a direct measure of the WF changes along the surface. While absolute WFs are difficult to extract, because of unknown STM tip conditions, the relative difference in the WF and the spatial extent of the WF modulation can be measured accurately, and this is the critical information required for the interface band alignment.

Figure 4 shows the dI/dV spectra and FER across a Pt_2Te_2/$PtTe_2$ interface. In dI/dV spectra the Fermi level is the reference energy at 0 eV, and thus the Fermi level of the metal is always aligned with the Fermi level in the semiconductor. What is important is the level of the semiconductor band edges at the metal contact and its comparison with the band edges before contact has been made, which presumably is the same

https://doi.org/10.1021/acs.nanolett.2c03715
Nano Lett. 2022, 22, 9571−9577

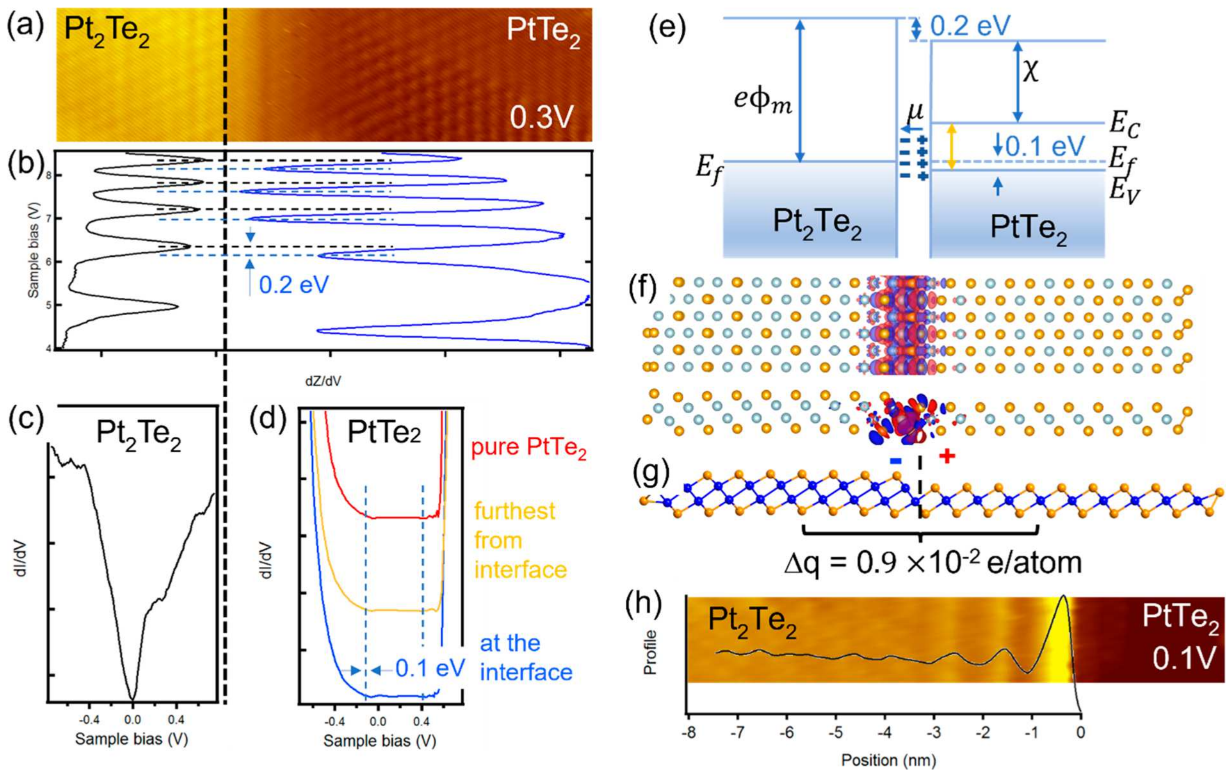

Figure 4. Determination of the electronic structure of the Pt_2Te_2−$PtTe_2$ metal/semiconductor interface by low temperature (20 K) STM/STS measurements and DFT. (a) Atomically resolved STM image of the interface. (b) Field emission resonance spectroscopy, showing a 0.2 eV lower WF of the semiconducting $PtTe_2$ compared to the metallic Pt_2Te_2 side of the heterojunction. (c) dI/dV spectra showing the metallic properties of Pt_2Te_2 and (d) a 0.5 eV band gap of $PtTe_2$. For $PtTe_2$, spectra of a pure $PtTe_2$ sample (without the presence of interfaces with Pt_2Te_2) are shown by the red spectrum, which indicates an intrinsic p-type doping level. The blue and yellow spectra are taken close and far away (∼10 nm) from the interface with Pt_2Te_2. All spectra show a very similar Fermi-level position and thus indicate a flat band alignment at the interface. (e) Schematic interface electronic structure derived from the STS data. The 0.2 eV WF offset between the metal and the semiconductor implies an interface dipole as indicated. (f) Charge densities derived from DFT calculations (red region = increase, blue region = decrease) indicating the atomic scale of the charge redistribution at the interface. Bader charge integration shown in (g) indicates that more electrons are "lost" (moved to the atoms exactly at the interface) from the $PtTe_2$ region than for the Pt_2Te_2 region, giving rise to the interface dipole. (h) STM images at low bias voltage across the Pt_2Te_2/$PtTe_2$ interface exhibit oscillation at the interface in the metallic Pt_2Te_2 phase. These oscillations may be associated with Friedel oscillations due to screening of the charges at the interface.

as far away from the contact. For an as grown pristine $PtTe_2$ film the dI/dV spectrum is shown in Figure 4d as the red spectrum. The calculated local density of states near the interface is presented in Figure S4, and it is in qualitative agreement with the experimental results. This film is p-type with the Fermi level ∼ 0.1 eV above the valence band edge. This band edge position is unaltered after contacting Pt_2Te_2, indicating that there is no significant shift of the Fermi level and thus no band bending or Schottky contact. The field emission resonance, shown in Figure 4b, on the other hand, indicates a shift of the WF across the interface by 0.2 eV. This shift is very sharp and occurs over less than a nanometer at the interface, indicating that the difference in the WF is accommodated by an interface dipole on the atomic scale. These measurements are summarized in an interface band diagram shown in Figure 4e. The calculated band edge positions relative to the vacuum level are shown in Figure S5 for the two materials. Consistent with the experiment, a shift of the WF by about 0.2 eV is needed to obtain the observed band alignment.

In the simplest model of a metal−semiconductor band alignment, the Schottky−Mott model, both the WF and Fermi level are aligned at the interface and the required band offset in the semiconductor to achieve this band alignment causes an extended charge depletion layer in the semiconductor. In contrast to metal−semiconductor contacts in 3D materials, the reduced charge screening in 2D materials is expected to give rise to a reduced charge equilibration process at 2D heterojunctions and a carrier delocalization.[39] Nevertheless, the WF offset measured here at the interface implies an atomic scale interface dipole. Interface dipoles can be caused for various reasons.[40] Spillover of metal Bloch states into the semiconducting gap (like surface dipoles on metal surfaces) would cause a dipole opposite to the one measured and thus can be excluded as the main reason for the dipole. Therefore, an atomic-scale charge transfer at the interface is most likely associated with this dipole. To get further insight into the charge redistribution at the interface, we carried out DFT calculations of the difference in the electronic charge upon contact formation. It should be pointed out that, contrary to the interface made form completely different materials, the Pt_2Te_2/$PtTe_2$ system can be split into separate Pt_2Te_2 and $PtTe_2$ semi-infinite sheets in several different ways, as shown in Figure S6, which gives rise to different binding energies between the subsystems and different charge transfers. For each division of the system, the charge transfer is confined to a few atom spaces at the interface, as illustrated in Figure 4f for the division giving the highest energy release upon interface

https://doi.org/10.1021/acs.nanolett.2c03715
Nano Lett. 2022, 22, 9571−9577

formation. To avoid the ambiguity related to the choice of the subsystems, we adopted another strategy to assess the charge redistribution. The Bader charges in the areas (four primitive cells for each material) close to the interface were calculated and compared to those in infinite $Pt_2Te_2/PtTe_2$ systems. The results indicated that the decrease in the electronic charge is larger in $PtTe_2$ system, giving rise to a difference of 0.9×10^{-2} e/atom, with positive charge accumulated in Pt_2Te_2, in agreement with the experimental data.

In general, excess charges at metal/semiconductor interfaces must be screened and give rise to Friedel oscillations. In this 2D system such Friedel oscillations may be imaged directly by STM. At low bias voltages oscillations are observed in STM images in the metallic Pt_2Te_2 along the interface as shown in Figure 4h, and these oscillations are consistent with the screening of the excess charges at the interface.

In conclusion, a compositional phase transformation in $PtTe_2$ is enabled by on-surface reaction with vapor deposited Pt. This implies that vapor deposition of Pt on monolayer $PtTe_2$ causes its transformation into metallic Pt_2Te_2 and a side-metal contact to semiconducting $PtTe_2$. We have shown that this configuration results in a barrier-less flat band configuration where the WF differences between the metal and the semiconducting part are compensated by an interface dipole at the atomic scale. Thus, the heterojunction between Pt_2Te_2 and $PtTe_2$ can be understood by a modified Schottky−Mott rule, with the only change being to replace the WF of the free metal edge with the new effective WF. The effective interface WF is the metal WF minus the interface dipole. Similar effective WFs due to interface dipoles were invoked in metal−graphene contacts.[41] Interestingly, this interface dipole is just large enough to allow for a flat band alignment and thus a barrier-less metal−semiconductor junction. However, the Fermi level of the metal lies within the semiconducting gap and thus does not pin the band edges. Thus, applications that allow shifting of the Fermi level in the semiconductor by gating may induce charge injection barriers. Such effects should be studied in future experiments by transport measurements and/or nano-beam photoemission studies. Enabling efficient charge injection into a material with large spin−orbit coupling like $PtTe_2$ is a prerequisite for making efficient spin and charge devices. The unique compositional transformation from one ordered 2D phase to another may play an important role in the development of future nanodevices. The process demonstrated here of transforming one 2D compound into another by on surface reaction with vapor deposited elements should not be limited to the Pt−telluride system only. Other 2D materials may be transformed by similar surface reactions and thus enable a new pathway for 2D material synthesis and formation of in-plane 2D heterojunctions.

ASSOCIATED CONTENT

Supporting Information

The Supporting Information is available free of charge at https://pubs.acs.org/doi/10.1021/acs.nanolett.2c03715.

Computational study of the reaction of excess Pt with PtTe2 and their diffusion barriers, comparison of formation energies of Pt_2Te_2 phase relative to Pt-cluster formation, additional STM studies of Pt_2Te_2 nucleation and growth, calculations of local density of states at $PtTe_2/Pt_2Te_2$ junction, calculated band edge energies relative to the vacuum level for $PtTe_2$ and Pt_2Te_2, computed charge transfer at $PtTe_2/Pt_2Te_2$ junctions, and experimental and computational details and methods (PDF)

AUTHOR INFORMATION

Corresponding Author

Matthias Batzill − *Department of Physics, University of South Florida, Tampa, Florida 33620, United States*; orcid.org/0000-0001-8984-8427; Email: mbatzill@usf.edu

Authors

Kinga Lasek − *Department of Physics, University of South Florida, Tampa, Florida 33620, United States*

Jingfeng Li − *Department of Physics, University of South Florida, Tampa, Florida 33620, United States*

Mahdi Ghorbani-Asl − *Institute of Ion Beam Physics and Materials Research, Helmholtz-Zentrum Dresden-Rossendorf, 01328 Dresden, Germany*; orcid.org/0000-0003-3060-4369

Salma Khatun − *Department of Physics, University of South Florida, Tampa, Florida 33620, United States*

Onyedikachi Alanwoko − *Department of Physics, University of South Florida, Tampa, Florida 33620, United States*; orcid.org/0000-0002-0683-4095

Vimukthi Pathirage − *Department of Physics, University of South Florida, Tampa, Florida 33620, United States*

Arkady V. Krasheninnikov − *Institute of Ion Beam Physics and Materials Research, Helmholtz-Zentrum Dresden-Rossendorf, 01328 Dresden, Germany; Department of Applied Physics, Aalto University, 00076 Aalto, Finland*; orcid.org/0000-0003-0074-7588

Complete contact information is available at: https://pubs.acs.org/10.1021/acs.nanolett.2c03715

Author Contributions

⊥(K.L. and J.L.) Contributed equally.

Notes

The authors declare no competing financial interest.

ACKNOWLEDGMENTS

Financial support through NSF Grant No. 2140038 is acknowledged. In addition, we acknowledge funding from the German Research Foundation (DFG), Project KR 4866/6-1, and through the collaborative research center "Chemistry of Synthetic 2D Materials" SFB-1415-417590517. We further thank the Gauss Centre for Super-computing e.V. (www.gauss-centre.eu) for providing computing time on the GCS Supercomputer HAWK at Höchstleistungsrechenzentrum Stuttgart (www.hlrs.de) and also TU Dresden (Taurus cluster) for generous grants of CPU time.

REFERENCES

(1) Lasek, K.; Li, J.; Kolekar, S.; Coelho, P. M.; Zhang, M.; Wang, Z.; Batzill, M.; Guo, L. Synthesis and Characterization of 2D Transition Metal Dichalcogenides: Recent Progress from a Vacuum Surface Science Perspective. *Surf. Sci. Rep.* **2021**, *76*, 100523.

(2) Cho, S.; Kim, S.; Kim, J. H.; Zhao, J.; Seok, J.; Keum, D. H.; Baik, J.; Choe, D.-H.; Chang, K. J.; Suenaga, K.; Kim, S. W.; Lee, Y. H.; Yang, H. Phase Patterning for Ohmic Homojunction Contact in $MoTe_2$. *Science* **2015**, *349*, 625−628.

(3) Lin, Y.-C.; Dumcenco, D. O.; Huang, Y.-S.; Suenaga, K. Atomic mechanism of the semiconducting-to-metallic phase transition in single-layered MoS_2. *Nat. Nanotechnol.* **2014**, *9*, 391−396.

(4) Acerce, M.; Voiry, D.; Chhowalla, M. Metallic 1T Phase MoS_2 Nanosheets as Supercapacitor Electrode Materials. *Nat. Nanotechnol.* **2015**, *10*, 313.
(5) Wypych, F.; Schöllhorn, R. 1T-MoS_2, a New Metallic Modification of Molybdenum Disulfide. *J. Chem. Soc., Chem. Commun.* **1992**, 1386−1388.
(6) Papageorgopoulos, C. A.; Jaegermann, W. Li intercalation across and along the van der Waals surfaces of MoS_2(0001). *Surf. Sci.* **1995**, *338*, 83−93.
(7) Kim, J. S.; Kim, J.; Zhao, J.; Kim, S.; Lee, J. H.; Jin, Y.; Choi, H.; Moon, B. H.; Bae, J. J.; Lee, Y. H.; Lim, S. C. Electrical Transport Properties of Polymorphic MoS_2. *ACS Nano* **2016**, *10*, 7500−7506.
(8) Kappera, R.; Voiry, D.; Yalcin, S. E.; Branch, B.; Gupta, G.; Mohite, A. D.; Chhowalla, M. Phase-Engineered Low-Resistance Contacts for Ultrathin MoS_2 Transistors. *Nat. Mater.* **2014**, *13*, 1128−1134.
(9) Duerloo, K.-A. N.; Li, Y.; Reed, E. J. Structural Phase Transitions in Two-Dimensional Mo- and W-Dichalcogenide Monolayers. *Nat. Commun.* **2014**, *5*, 4214.
(10) Wang, Z.; Sun, Y.-Y.; Abdelwahab, I.; Cao, L.; Yu, W.; Ju, H.; Zhu, J.; Fu, W.; Chu, L.; Xu, H.; Loh, K. P. Surface-Limited Superconducting Phase Transition on 1T-TaS_2. *ACS Nano* **2018**, *12*, 12619−12628.
(11) Arnold, F.; Stan, R.-M.; Mahatha, S. K.; Lund, H. E.; Curcio, D.; Dendzik, M.; Bana, H.; Travaglia, E.; Bignardi, L.; Lacovig, P.; Lizzit, D.; Li, Z.; Bianchi, M.; Miwa, J. A.; Bremholm, M.; Lizzit, S.; Hofmann, P.; Sanders, C. E. Novel Single-Layer Vanadium Sulphide Phases. *2D Mater.* **2018**, *5*, 045009.
(12) Sutter, E.; Huang, Y.; Komsa, H.-P.; Ghorbani-Asl, M.; Krasheninnikov, A. V.; Sutter, P. Electron-Beam Induced Transformations of Layered Tin Dichalcogenides. *Nano Lett.* **2016**, *16*, 4410−4416.
(13) Zhu, H.; Wang, Q.; Zhang, C.; Addou, R.; Cho, K.; Wallace, R. M.; Kim, M. J. New Mo_6Te_6 Sub-Nanometer-Diameter Nanowire Phase from 2H-$MoTe_2$. *Adv. Mater.* **2017**, *29*, 1606264.
(14) Oyedele, A. D.; Yang, S.; Feng, T.; Haglund, A. V.; Gu, Y.; Puretzky, A. A.; Briggs, D.; Rouleau, C. M.; Chisholm, M. F.; Unocic, R. R.; Mandrus, D.; Meyer, H. M., III; Pantelides, S. T.; Geohegan, D. B.; Xiao, K. Defect-Mediated Phase Transformation in Anisotropic Two-Dimensional PdSe2 Crystals for Seamless Electrical Contacts. *J. Am. Chem. Soc.* **2019**, *141*, 8928−8936.
(15) Li, J.; Kolekar, S.; Ghorbani-Asl, M.; Lehnert, T.; Biskupek, J.; Kaiser, U.; Krasheninnikov, A. V.; Batzill, M. Layer-Dependent Band Gaps of Platinum Dichalcogenides. *ACS Nano* **2021**, *15*, 13249−13259.
(16) Gimpl, M. L.; Nelson, C. E.; Fuschillo, N. Some Properties of Platinum Monotelluride (PtTe). *Am. Mineral.* **1963**, *48*, 689−691.
(17) Thomassen, L. Ueber Kristallstrukturen einiger Binaerer Verbindungen der Platinmetalle. *Z. Phys. Chem. B* **1929**, *2*, 349−379.
(18) Cenzual, K.; Gelato, L. M.; Penzo, M.; Parthé, E. Overlooked Triagonal Symmetry in Structures Reported with Monoclinic Centered Bravais Lattices, Trigonal Description of Li_8Pb_3, PtTe, Pt_3Te_4, Pt_2Te_3, $LiFe_6Ge_4$, $LiFe_6Ge_5$, $CaGa_6Te_{10}$, and $La_{3.266}Mn_{1.1}S_6$. *Zeitschr. Kristallogra.* **1990**, *193*, 217−242.
(19) Li, J.; Kolekar, S.; Xin, Y.; Coelho, P. M.; Lasek, K.; Nugera, F. A.; Gutiérrez, H. R.; Batzill, M. Thermal Phase Control of Two-Dimensional Pt-Chalcogenide (Se and Te) Ultrathin Epitaxial Films and Nanocrystals. *Chem. Mater.* **2021**, *33*, 8018−8027.
(20) Coelho, P. M.; Komsa, H. P.; Diaz, H. C.; Ma, Y.; Krasheninnikov, A. V.; Batzill, M. Post-Synthesis Modifications of Two-Dimensional $MoSe_2$ or $MoTe_2$ by Incorporation of Excess Metal Atoms into the Crystal Structure. *ACS Nano* **2018**, *12*, 3975−3984.
(21) Batzill, M. Mirror Twin Grain Boundaries in Molybdenum Dichalcogenides. *J. Phys.: Condens. Matter* **2018**, *30*, 493001.
(22) Coelho, P. M.; Komsa, H. P.; Lasek, K.; Kalappattil, V.; Karthikeyan, J.; Phan, M. H.; Krasheninnikov, A. V.; Batzill, M. Room-Temperature Ferromagnetism in $MoTe_2$ by Post-Growth Incorporation of Vanadium Impurities. *Adv. Electr. Mater.* **2019**, *5*, 1900044.
(23) Karthikeyan, J.; Komsa, H. P.; Batzill, M.; Krasheninnikov, A. V. Which Transition Metal Atoms can be Embedded into Two-Dimensional Molybdenum Dichalcogenides and Add Magnetism? *Nano Lett.* **2019**, *19*, 4581−4587.
(24) Yan, M.; Huang, H.; Zhang, K.; Wang, E.; Yao, W.; Deng, K.; Wan, G.; Zhang, H.; Arita, M.; Yang, H.; Sun, Z.; Yao, H.; Wu, Y.; Fan, S.; Duan, W.; Zhou, S. Lorentz-Violating Type-II Dirac Fermions in Transition Metal Dichalcogenide $PtTe_2$. *Nat. Commun.* **2017**, *8*, 257.
(25) Lin, M.-K.; Villaos, R. A. B.; Hlevyack, J. A.; Chen, P.; Liu, R.-Y.; Hsu, C.-H.; Avila, J.; Mo, S.-K.; Chuang, F.-C.; Chiang, T. C. Dimensionality-Mediated Semimetal-Semiconductor Transition in Ultrathin $PtTe_2$ Films. *Phys. Rev. Lett.* **2020**, *124*, 036402.
(26) Zhang, L.; Yang, T.; Arramel; Feng, Y. P.; Wee, A. T. S.; Wang, Z. MBE-Grown Ultrathin $PtTe_2$ Film and the Layer-Dependent Electronic Structure. *Nanoscale* **2022**, *14*, 7650−7658.
(27) Kwon, G.; Choi, Y.-H.; Lee, H.; Kim, H.-S.; Jeong, J.; Jeong, K.; Baik, M.; Kwon, H.; Ahn, J.; Lee, E.; Cho, M.-H. Interaction- and Defect-Free van der Waals Contacts Between Metals and Two-Dimensional Semiconductors. *Nat. Electr.* **2022**, *5*, 241−247.
(28) Wang, Y.; Kim, J. C.; Wu, R. Y.; Martinez, J.; Song, X.; Yang, J.; Zhao, F.; Mkhoyan, A.; Jeong, H. Y.; Chhowalla, M. Van der Waals Contacts Between Three-Dimensional Metals and Two-Dimensional Semiconductors. *Nature* **2019**, *568*, 70−74.
(29) Liu, Y.; Guo, J.; Zhu, E.; Liao, L.; Lee, S.-J.; Ding, M.; Shakir, I.; Gambin, V.; Huang, Y.; Duan, X. Approaching the Schottky−Mott Limit in van der Waals Metal−Semiconductor Junctions. *Nature* **2018**, *557*, 696−700.
(30) Song, S.; Sim, Y.; Kim, S.-Y.; Kim, J. H.; Oh, I.; Na, W.; Lee, D. H.; Wang, J.; Yan, S.; Liu, Y.; Kwak, J.; Chen, J.-H.; Cheong, H.; Yoo, J.-W.; Lee, Z.; Kwon, S.-Y. Wafer-Scale Production of Patterned Transition Metal Ditelluride Layers for Two-Dimensional Metal−Semiconductor Contacts at the Schottky−Mott Limit. *Nat. Electr.* **2020**, *3*, 207−215.
(31) Allain, A.; Kang, J.; Banerjee, K.; Kis, A. Electrical Contacts to Two-Dimensional Semiconductors. *Nat. Mater.* **2015**, *14*, 1195−1205.
(32) Joshi, S.; Ecija, D.; Koitz, R.; Iannuzzi, M.; Seitsonen, A. P.; Hutter, J.; Sachdev, H.; Vijayaraghavan, S.; Bischoff, F.; Seufert, K.; Barth, J. V.; Auwärter, W. Boron Nitride on Cu(111): An Electronically Corrugated Monolayer. *Nano Lett.* **2012**, *12*, 5821−5828.
(33) Zhang, Q.; Yu, J.; Ebert, P.; Zhang, C.; Pan, C.-R.; Chou, M.-Y.; Shih, C.-K.; Zeng, C.; Yuan, S. Tuning Band Gap and Work Function Modulations in Monolayer hBN/Cu(111) Heterostructures with Moiré Patterns. *ACS Nano* **2018**, *12*, 9355−9362.
(34) Wang, B.; Caffio, M.; Bromley, C.; Früchtl, H.; Schaub, R. Coupling Epitaxy, Chemical Bonding, and Work Function at the Local Scale in Transition Metal-Supported Graphene. *ACS Nano* **2010**, *4*, 5773−5782.
(35) Rienks, E. D. L.; Nilius, N.; Rust, H.-P.; Freund, H.-J. Surface Potential of a Polar Oxide Film: FeO on Pt(111). *Phys. Rev. B* **2005**, *71*, 241404.
(36) Lichtenstein, L.; Heyde, M.; Ulrich, S.; Nilius, N.; Freund, H.-J. Probing the Properties of Metal−Oxide Interfaces: Silica Films on Mo and Ru Supports. *J. Phys.: Condens. Matter* **2012**, *24*, 354010.
(37) Ploigt, H. C.; Brun, C.; Pivetta, M.; Patthey, F.; Schneider, W.-D. Local Work Function Changes Determined by Field Emission Resonances: NaCl/Ag(100). *Phys. Rev. B* **2007**, *76*, 195404.
(38) Ruggiero, C. D.; Choi, T.; Gupta, J. A. Tunneling Spectroscopy of Ultrathin Insulating Films: CuN on Cu(100). *Appl. Phys. Lett.* **2007**, *91*, 253106.
(39) Yu, H.; Kutana, A.; Yakobson, B. I. Carrier Delocalization in Two-Dimensional Coplanar p−n Junctions of Graphene and Metal Dichalcogenides. *Nano Lett.* **2016**, *16*, 5032−5036.
(40) Ling, S.; Watkins, M. B.; Shluger, A. L. Effects of Atomic Scale Roughness at Metal/Insulator Interfaces on Metal Work Function. *Phys. Chem. Chem. Phys.* **2013**, *15*, 19615−19624.

(41) Giovannetti, G.; Khomyakov, P. A.; Brocks, G.; Karpan, V. M.; van den Brink, J.; Kelly, P. J. Doping Graphene with Metal Contacts. *Phys. Rev. Lett.* **2008**, *101*, 026803.

https://doi.org/10.1021/acs.nanolett.2c03715
Nano Lett. 2022, 22, 9571−9577